Dynamic Responses and Wake Characteristics of a Floating Offshore Wind Turbine in Yawed Conditions

Shun Xu*, Weiwen Zhao* and Decheng Wan*†
Computational Marine Hydrodynamic Lab (CMHL), School of Naval Architecture, Ocean and Civil Engineering
Shanghai Jiao Tong University, Shanghai, China

Yan Zhao
Key Laboratory of Far-Shore Wind Power Technology of Zhejiang Province
Huadong Engineering Corporation Limited, Hangzhou, China

Numerical simulations of a floating offshore wind turbine (FOWT) in yawed conditions are carried out using a coupled large eddy simulation and aero-hydro-moor-servo dynamics code. The inflow wind is an atmospheric boundary layer inflow simulated by large eddy simulation with a long duration. Two scenarios with yaw angles of 15° and 30° for a wind turbine are investigated, and the aerodynamics, hydrodynamics, and wake characteristics are compared against a non-yaw scenario. The study concludes that as the yaw angle increases, the rotor power of FOWT decreases. However, the rotor thrust of the 15° yaw angle is slightly higher compared with the non-yaw scenario. In terms of platform motions, there is minimal disparity for surge and pitch between the 15° yaw angle and non-yaw conditions. When the yaw angle is 30°, both surge and pitch are notably reduced. The sway increases with the yaw angle because of the crosswise component of rotor thrust. Furthermore, we observe a faster wake recovery and more pronounced wake deflection with an increasing yaw angle. These observations have a positive impact on the inflow wind condition and power generation of downstream wind turbines.

INTRODUCTION

In recent years, wind energy has become a hot topic because of its advantages of nonpollution and renewable and rich resources (Rohrig et al., 2019). The wind energy harvesting consists of two parts: onshore and offshore. Offshore wind energy, unlike onshore, offers richer resources and is not hindered by land and noise limitations (Li et al., 2020). Most wind resources are distributed in a deep water area—specifically, with over 80% of offshore wind potential in areas deeper than 60 m. The bottom-fixed offshore wind turbine is not feasible for the deep water scenario because the construction cost of the bottom foundation will increase dramatically with water depth, which is commercially expensive and impractical. A potential solution is transitioning from fixed foundations to floating ones. Consequently, the design and development of a floating offshore wind turbine (FOWT) are essential to harvest the wind resources in the deep water area and ensure commercial feasibility (Ramachandran et al., 2022).

In contrast to the prototype and scale-down basin experiment, the numerical simulation of FOWT offers cost effectiveness, especially with advances in high-performance computers. Therefore, the numerical simulation becomes a powerful and indispensable tool for the design and development of FOWT. To yield accurate analysis results and support the design of FOWT, Tran and Kim (2016) proposed a high-fidelity computational model using an overset mesh technique. Their results for unsteady aerodynamics, platform hydrodynamics, and mooring forces showed good

agreement with the test data and numerical results calculated by the NREL FAST code. Similarly, Zhang and Kim (2018) utilized overset mesh in STAR-CCM+ for high-fidelity analysis of a semisubmersible FOWT. Their findings indicated a 7.8% increase in rotor thrust but a 10% decrease in rotor power compared with an onshore wind turbine.

The high-fidelity overset mesh technique is computationally expensive and time-consuming (Xu et al., 2022), limiting its further application in the numerical analysis of FOWT. Troldborg et al. (2007) pointed out that the actuator line model (ALM) used for wind turbine aerodynamics can improve the computational efficiency. The ALM treats the wind turbine as a body force and guarantees accuracy by solving the Navier-Stokes equations. Cheng et al. (2019) developed an aero-hydrodynamic model of FOWT—namely, FOWT-UALM-SJTU—by combining the ALM and an in-house two-phase computational fluid dynamics (CFD) solver. They introduced an additional velocity to the conventional ALM due to the motions of floating platform. By using the well-validated FOWT solver FOWT-UALM-SJTU, Huang and Wan (2019) presented a systematic study on the interaction between the wind turbine and floating platform. Their results highlighted significant changes in the local angle of attack from the surge and pitch motions of a floating platform. After that, Huang et al. (2021) developed an aero-hydro-elastic numerical framework of FOWT. The elastic ALM accounts for the blade deformation of FOWT, integrating the additional velocity induced by blade deformation and the one-dimensional finite element structure model.

Among the above numerical studies of FOWT, the inflow wind conditions were simplified (i.e., the uniform or shear wind inflows). However, the FOWT operates in an atmospheric boundary layer (ABL) wind field, where the wind inflow is definitely turbulent. As the wind turbine diameter increases, the effects of turbulence wind on the aerodynamic performance of FOWT become more pronounced. Li et al. (2018) investigated the effects of the ABL wind field on the aerodynamics of a FOWT, finding that power generation is sensitive to the ABL wind field.

Xu, Zhuang, et al. (2023) explored the aerodynamic responses and wake characteristics of FOWT in an ABL wind field. Their results revealed that atmospheric turbulence has a greater influence on power variation than platform motions. Zhou et al. (2022) examined how different inflow wind conditions (turbulent, shear, and uniform) affect aerodynamics and the platform motions of a semisubmersible FOWT. What's more, Doubrawa et al. (2019) investigated the fatigue loads of a spar-type FOWT in ABL wind fields. They generated turbulent wind fields through both large eddy simulation (LES) and a synthetic turbulent wind model and then compared and analyzed results obtained from different methods of generating turbulent wind.

In addition to the high turbulence, another significant feature of the ABL wind field is that it is nonstationary (Porté-Agel et al., 2020), involving frequent changes in wind direction. Consequently, the yaw operation of FOWT is a common situation. However, most of the numerical studies of FOWT focus on the non-yaw scenario, where the wind direction is perpendicular to the rotation plane of wind turbine. When the inflow wind direction changes, the aerodynamic performance, platform hydrodynamic responses, and wake characteristics are significantly changed. This emphasizes the necessity for systematic investigation into the dynamic responses of yawed FOWT.

In this study, we present the numerical investigations of a yawed FOWT immersed in the ABL wind fields by using a coupled LES and aero-hydro-moor-servo dynamics code. This coupled model can obtain a reliable and realistic wake of FOWT with acceptable computational cost, which makes it possible to explore the far-wake characteristics of FOWT and wake interactions between multi-FOWTs. Specifically, the LES with sufficient simulation duration is employed to generate the ABL turbulent wind inflow. The ALM is applied to predict the aerodynamic performance and wake characteristics of FOWT, whereas the coupled dynamic responses of FOWT are predicted by the NREL FAST code. A comparative analysis of aerodynamic performance, platform motions, and wake characteristics of FOWT is conducted between yawed and non-yaw scenarios across various yaw angles.

NUMERICAL METHODS

Governing Equations

To better simulate the turbulence in the ABL wind field and analyze the characteristics in the wind turbine wake, the LES is used for the simulations of ABL wind field and FOWT. The spatial filtered governing equations, including the continuity equation and momentum equation, are presented as follows:

$$\frac{\partial \bar{u}_i}{\partial x_i} = 0 \tag{1}$$

$$\frac{\partial \bar{u}_i}{\partial t} + \frac{\partial}{\partial x_j}(\bar{u}_j \bar{u}_i) = -\underbrace{\frac{\partial \hat{p}}{\partial x_i}}_{\text{I}} - \underbrace{\frac{1}{\rho_0}\frac{\partial}{\partial x_i}\bar{p}_0(x, y)}_{\text{II}} - \underbrace{2\varepsilon_{i3k}\Omega_3 \bar{u}_k}_{\text{III}}$$
$$- \underbrace{\frac{\partial}{\partial x_j}\left(\tau_{ij}^D\right)}_{\text{IV}} + \underbrace{\frac{1}{\rho_0}f_i^T}_{\text{V}} \tag{2}$$

where the overbar denotes the spatial filtered value; subscript $i = 1, 2, 3$ is the component along the x, y, or z axis, respectively. In the momentum equation, Term I is the modified pressure gradient; the modified pressure $\hat{p}$ consists of two parts: the resolved pressure subtracting the background driving pressure normalized by ρ and one-third of the stress tensor trace (i.e., $\hat{p} = (\bar{p} - p_0 + \rho g z)/\rho + \tau_{kk}/3$). Term II is the background pressure

gradient, aiming to drive the wind field to a desired wind speed at specified height. Term III is the Coriolis force, reflecting the influence of earth's rotation on the ABL wind field. Term IV is the tensor of fluid stress induced by the turbulence model of LES; the Smagorinsky subscale model (Smagorinsky, 1963) is used to calculate the stress and closure of the momentum equation. Term V is a source term of body force on the wind turbine blade, which is needed when the wind turbine is introduced into the wind field and used to consider the effect of the wind turbine on the flow field. Note that the viscous stress is neglected because of the high Reynolds number feature of the ABL wind field. More details of the governing equations can be obtained in Churchfield, Lee, Michalakes, et al. (2021).

Actuator Line Model

Different from the blade-resolved overset mesh technique, the wind turbine modeled by ALM can significantly save the computational cost, whereas numerical accuracy is guaranteed by solving the governing equations of the flow field. The ALM was originally proposed by Sørensen and Shen (2002), and the idea behind this method is to regard the wind turbine as a body force in the flow field. The wind turbine blades are divided into many blade elements radially, and the blade element theory is used to calculate the aerodynamic force of each blade element. To account for the turbine's impact on the flow field, the forces of blade elements are imposed on the flow field via a source term of body force added to the momentum equation. Figure 1 shows velocity vector analysis of a two-dimensional airfoil. The relative inflow velocity U_{rel} is determined by

$$U_{\text{rel}} = \sqrt{(U_z + U_{M,Z})^2 + (\Omega r - U_\theta + U_{M,\theta})^2} \tag{3}$$

where U_z and U_θ are the axial and tangential components of inflow wind velocity, respectively; $U_{M,Z}$ and $U_{M,\theta}$ are the respective axial and tangential components of additional velocity U_M, which is induced by platform motions; Ω is the rotor speed; and r is the radial distance from blade element to rotor center.

The aerodynamic force of a blade element is calculated by

$$f = (L, D) = \frac{1}{2}\rho U_{\text{rel}}^2 c\, dr(C_L \vec{e_L} + C_D \vec{e_D}) \tag{4}$$

where L and D are the lift and drag forces of blade element, respectively; ρ is the air density; c is the chord length of a two-dimensional airfoil; dr is the width of the blade element; C_L and C_D are the coefficients of lift and drag forces, respectively; and $\vec{e_L}$ and $\vec{e_D}$ are the unit vectors of lift and drag forces, respectively.

The coefficients of lift and drag forces are determined by a local angle of attack α. This angle is calculated as the difference between the local angle of inflow ϕ and local angle of pitch γ.
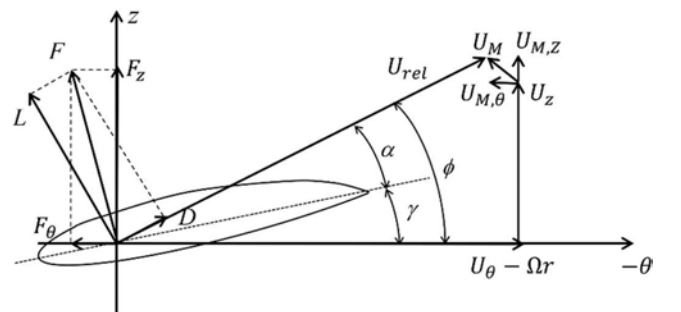

Fig. 1 Velocity vectors of a two-dimensional airfoil

The local angle of inflow ϕ is determined by the inflow wind condition.

The numerical singularity occurs when the aerodynamic forces of blade elements are directly imposed on a flow field. Therefore, we use the Gauss kernel function to smooth the body force of a wind turbine. The smoothed body force is expressed by

$$f_\varepsilon = f \otimes \eta_\varepsilon = \sum_{i=1}^{N} f_i(x_i, y_i, z_i, t) \frac{1}{\varepsilon^3 \pi^{3/2}} \exp\left[-\left(\frac{d_i}{\varepsilon}\right)^2\right] \qquad (5)$$

where N is the number of blade elements of a turbine blade, (x_i, y_i, z_i) is the position of the ith blade element, d_i is the distance between the blade element and projection position, ε is the projection width, $\varepsilon \approx 2\Delta x$ (Troldborg, 2009) is recommended to ensure numerical stability, and Δx is the mesh size near the blade element.

Simulation Procedure

A coupled LES and aero-hydro-moor-servo dynamics code is used in this work. This code was proposed and implemented in the NREL SOWFA framework (Churchfield, Lee, and Moriarty, 2012), a LES solver for numerical simulations of a large wind farm based on open-source OpenFOAM CFD framework (Jasak et al., 2007). The simulation procedure of a yawed FOWT immersed in an ABL wind field is shown in Fig. 2. First, the LES with sufficient simulation duration (18,600 s) is used to develop the quasi-equilibrium ABL wind field. The data of last 600 s of upstream boundary are saved as the inflow wind condition of the yawed FOWT. The wind turbine blades are modeled by the ALM, and the wake is simulated in the LES framework. The fully coupled aero-hydro-moor-servo dynamics of FOWT are simulated and predicted by the NREL FAST code (Jonkman and Buhl, 2005) (version 8.16). The coupling between the LES framework and FAST code is implemented by delivering the CFD-solved wind velocity of the blade element and the FAST-solved position of the blade element to each other. Notably, this coupling is developed and proposed by NREL SOWFA, not in this work. This coupled code has been widely used for simulations of a wind turbine under ABL inflow (Johlas et al., 2021; Chanprasert et al., 2022). Because the wind velocity on a blade element is solved by the ALM in the LES framework, the momentum part of blade element momentum theory is neglected in the FAST code for wind turbine aerodynamics. Additionally, the numerical methods pertaining to the aero-hydro-moor-servo dynamics of FOWT are not presented, as this work utilizes a baseline and built-in case of FOWT within FAST. We believe that the numerical methods of
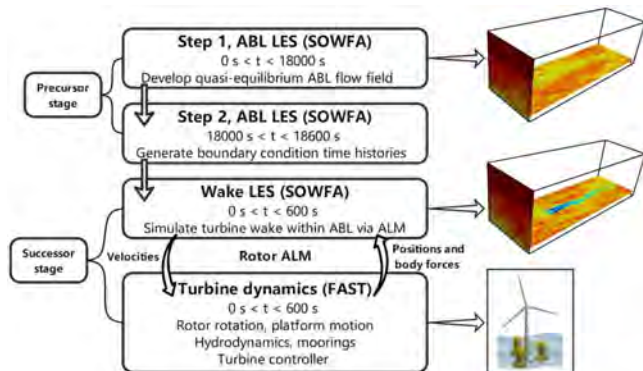
Term	Value
Rated power	5 MW
Rated wind velocity	11.4 m/s
Rated rotor velocity	12.1 rpm
Hub height	90 m
Orientation	Upwind
Blade number	3

Table 1   Gross properties of an NREL 5MW wind turbine

FOWT employed in FAST can be readily accessed in its theory guide (National Renewable Energy Laboratory, 2022).

SIMULATION CASES

Wind Turbine Model

This study employs the NREL 5MW wind turbine (Jonkman et al., 2009) mounted on the OC4 semisubmersible floating platform (Robertson et al., 2014) as the FOWT model, as shown in Fig. 3. The wind turbine is a conventional upwind wind turbine with three blades. The gross properties are summarized in Table 1. There are three controllers available for this wind turbine: torque controller, blade pith controller, and yaw controller. As this study focuses on the effect of yaw operation on dynamic responses and wake characteristics of FOWT, the yaw controller module in FAST remains inactive.

The OC4 DeepCwind semisubmersible floating platform is adopted to support the wind turbine. The floating platform is composed of three main offset columns, one central column, and some diagonal cross and horizontal bracing components. To limit the hydrodynamic responses of a floating platform, a mooring system with three mooring lines was used. The offset angle between two adjacent mooring lines is 120°, as shown in Fig. 4. Note that only the wind turbine is in yaw operation; the orientation of floating platform and mooring system is not changed. Specifically, the initial configuration of mooring line #2 aligns with the inflow direction of the combined wind-wave. The overall parameters of the floating platform and mooring system are concluded in Table 2.

Simulation of an ABL Wind Field

The ABL wind field is simulated by the LES with sufficient simulation duration. The computational domain is a cuboid with
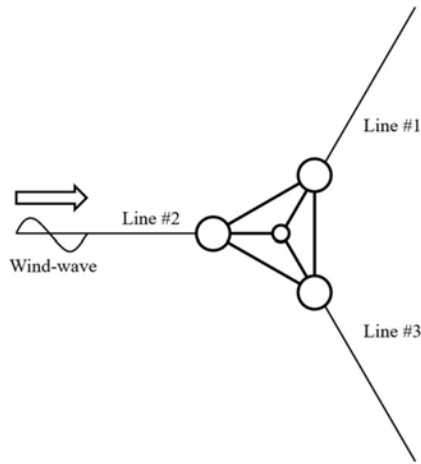

Fig. 2 Simulation procedure of FOWT immersed in an ABL wind field

Fig. 3 Overview of the FOWT model

Fig. 4 Orientation of floating platform and mooring system

Term	Value
Draft	20 m
Platform mass	13,473,000 kg
Displacement	13,986.8 m³
Center of mass	(0 m, 0 m, −13.5 m)
Platform roll inertia	6.827×10^9 kg·m²
Platform pitch inertia	6.827×10^9 kg·m²
Platform yaw inertia	1.226×10^{10} kg·m²
Depth to anchor	200 m
Depth to fairlead	14 m
Mooring line diameter	0.0766 m
Equivalent line mass density	113.35 kg/m
Equivalent mooring line extensional stiffness	753.6 MN

Table 2　Gross properties of floating platform and mooring system

dimensions of 3,000 m in length, 1,000 m in width, and 1,000 m in height, as shown in Fig. 5. The entire domain maintains a uniform mesh resolution of 10 m × 10 m × 10 m in the x, y, and z axes, totaling 3 million cells. Cyclic boundaries are employed on the four vertical boundaries, indicating that the wind field downstream will re-enter the upstream. The top boundary is a slip condition, implying no vertical velocity gradient at this level. The
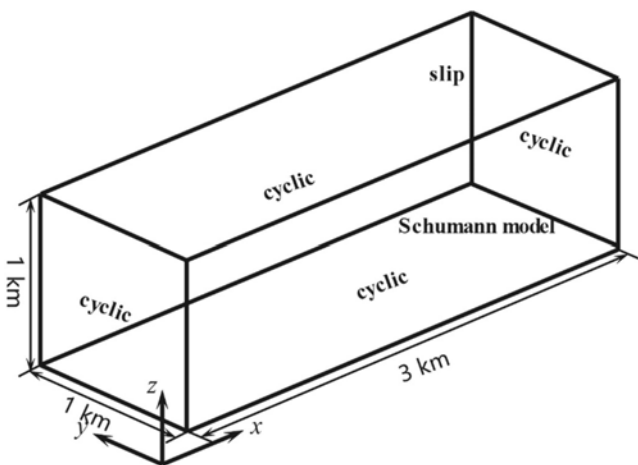
Schumann wall stress model (Schumann, 1975) is employed at the bottom boundary to calculate surface stress, with a surface roughness value of 0.001 chosen to represent a typical sea surface condition (Churchfield, Lee, Michalakes, et al., 2012; Bai et al., 2023; Wei et al., 2023). The initial wind condition is uniform wind with a velocity of 11.4 m/s throughout the domain, including the boundaries. The simulation time is 18,600 s to generate the quasi-equilibrium ABL wind field, and the time step is 0.2 s. The data of last 600 s from upstream boundary are saved as the inflow condition of the FOWT.

Simulation of FOWT

For the simulation of FOWT within the LES framework, the computational domain and background mesh resolution are the same as those used for the simulation of the ABL wind field—specifically, 3 km × 1 km × 1 km in size and 10 m × 10 m × 10 m in resolution. Figure 6 shows the computational domain and mesh refinement of the simulation of FOWT. The wind turbine is positioned downstream 800 m from the upstream inflow boundary (indicated by the black line). To capture the vortices in wind turbine wakes, we employ a two-level mesh refinement of the cuboid region. The length, width, and height of the first-level refinement region are $13D$, $4D$, and $3D$, respectively, where $D = 126$ m is the rotor diameter. The distance between the wind turbine and upstream boundary of the first-level refinement region is $3D$. The first-level refinement region's size is decreased by $2D$, $1D$, and $1D$ inwards along three respective directions, forming the second-level refinement region. After the mesh refinement, the mesh resolution near the wind turbine is 2.5 m × 2.5 m × 2.5 m, and the total mesh number is 12 million.

In comparison to the boundary conditions of the ABL wind field, the upstream inflow boundary of simulation of FOWT is changed to a mapping boundary condition. This implies that the time histories of data saved from the ABL wind field serve as the inflow condition of the simulation of FOWT. What's more, the zero gradient condition is applied on the downstream boundary to enable the fluid to exit freely. The flow field of wind turbine simulation is initialized using the ABL wind field at a time instant of 18,000 s. The simulation time of FOWT is 600 s, and the time step is 0.02 s to limit the blade tip from advancing more than one grid at one time step. In the result analysis, we exclude the first 200 s data of numerical results to eliminate the influence of a transient start-up of a wind turbine.

Fig. 5 Computational domain and boundary conditions of simulation of an ABL wind field
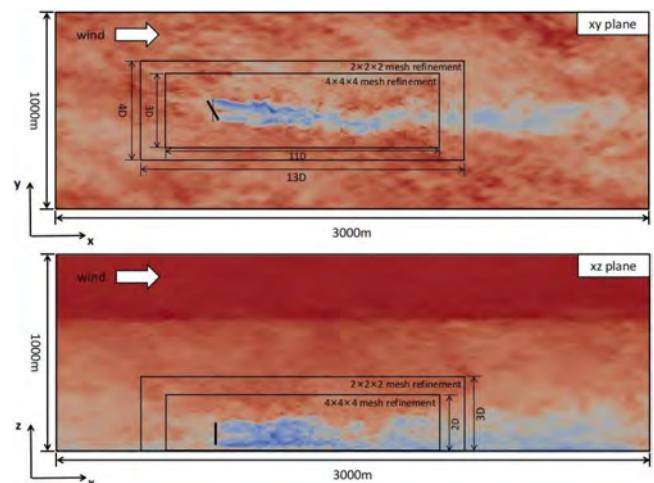

Fig. 6 Computational domain and mesh refinement of simulation of FOWT

The fully coupled aero-hydro-moor-servo dynamics of FOWT is simulated and predicted by the NREL FAST code. Note that the wind velocity of FOWT is solved and sampled in the LES framework. Therefore, the momentum part of blade element momentum theory used in the AeroDyn module is replaced by the ALM, and the InflowWind module used for the generation of the inflow wind condition remains inactive. The simulation time in FAST is 600 s, whereas the time step is 0.005 s, which means one time step of the LES framework contains four time iterations of FAST simulation.

For the combined wind-wave condition of FOWT, the simulated wind field from the LES framework is used. This wind inflow features a shear profile with a mean wind speed at a hub height of 11.4 m/s. The time-averaged characteristics of inflow wind are presented and analyzed in the following section. The incident wave is a Stokes first-order regular wave with a wave height of 7.58 m and period of 12.1 s. Two yaw angles, 15° and 30°, are applied to the wind turbine, and the results are compared with those of the non-yaw scenario. To clarify, the cases are named $\theta_{yaw} = 0°$, $\theta_{yaw} = 15°$, and $\theta_{yaw} = 30°$. It is noteworthy again that only the wind turbine is in yaw operation; the orientation of floating platform and mooring system remains aligned with the non-yaw scenario. Specifically, the initial configuration of mooring line #2 aligns with the inflow direction of the combined wind-wave, as shown in Fig. 4.

VALIDATION AND VERIFICATION

ABL Wind Field

The ABL wind field is simulated by the LES with sufficient simulation duration for the inflow wind condition of FOWT. Figure 7 shows the time-averaged profiles, including the wind speed and turbulence intensity (TI). The turbulence intensity is calculated by (Ning and Wan, 2019; Xu, Wang, et al., 2023):

$$TI_i(z) = \frac{\sqrt{\overline{(U_i(z) - \bar{U}_i(z))^2}}}{U_0} \tag{6}$$

where the overbar is the time average, $U_i(z)$ is the wind speed at height z ($i = x, y, z$), and U_0 is the rated wind velocity of 11.4 m/s. The wind speed at hub height is 11.4 m/s, and the wind profile shows good agreement with the logarithmic law, indicating that the desired atmosphere inflow profile is reproduced. The turbulence intensity decreases with height, and the x-axis component being more pronounced than the other two directions. Specifically, at hub height, the three components of turbulence intensity are 5.78, 3.82, and 1.85.

In addition to the time-averaged profiles presented here, the power spectrum of velocity fluctuations including three components was validated and analyzed in our previous work; for more details, refer to Xu, Zhuang, et al. (2023).

Mesh Convergence

To evaluate the sensitivity of numerical results to mesh generation, three different mesh resolutions near wind turbines are used: 3 m × 3 m × 3 m (coarse), 2.5 m × 2.5 m × 2.5 m (medium), and 2 m × 2 m × 2 m (fine). For simplicity of simulation, the uniform inflow with a wind speed of 11.4 m/s is utilized. The incident wave is a Stokes first-order regular wave with a wave
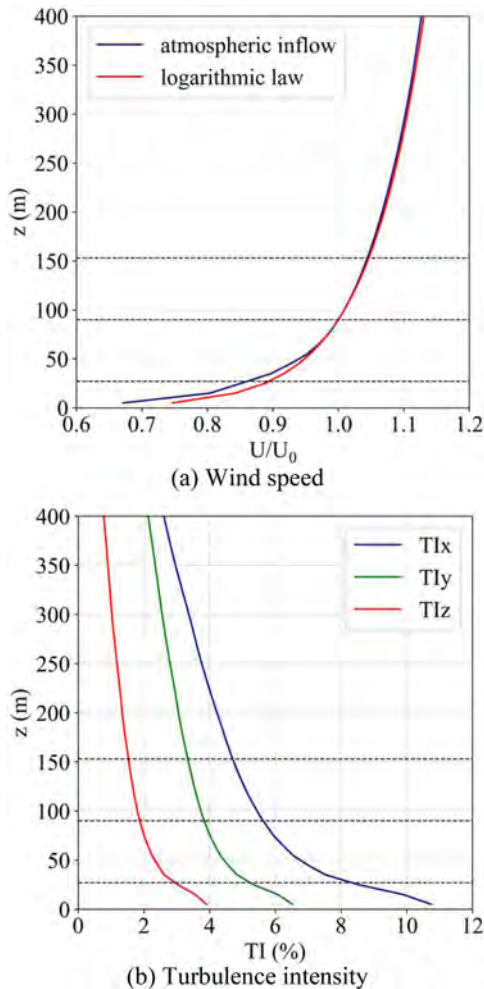
Fig. 7 Time-averaged profiles of the ABL wind field simulated by the LES; the three dashed lines denote the top, middle, and bottom of the rotor area.
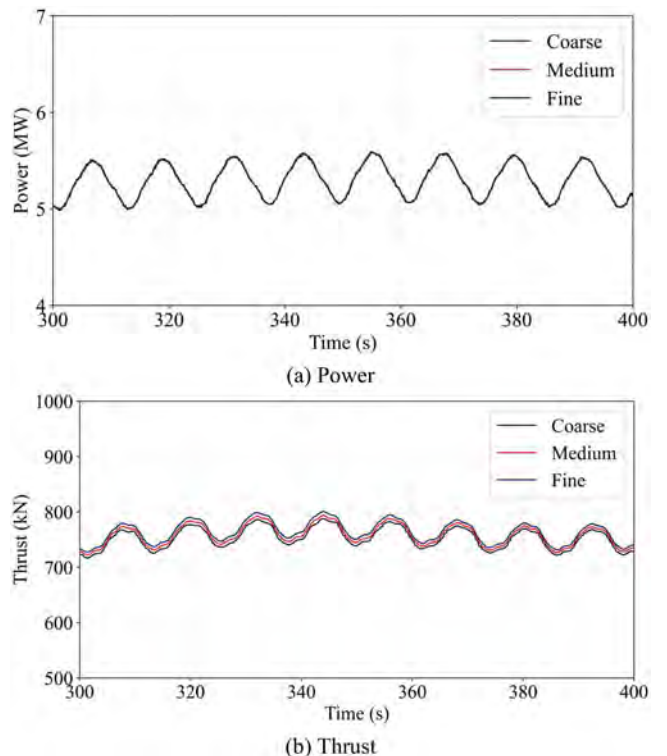
Fig. 8 Power and thrust of FOWT under three different mesh resolutions

height of 7.58 m and period of 12.1 s. Figure 8 shows the power and thrust of FOWT under three different mesh resolutions. A minor difference of power and thrust among these scenarios is observed, indicating that the numerical results are convergent in these mesh resolutions. What's more, the mesh resolution of 2.5 m × 2.5 m × 2.5 m is sufficient to capture and explore the characteristics in wind turbine wake (Churchfield, Lee, Michalakes, et al., 2021). As a result, the mesh resolution of 2.5 m × 2.5 m × 2.5 m near a wind turbine is used for result analysis.

Unsteady Aerodynamic Performance

The aerodynamic performance of FOWT exhibits a significant unsteady feature as a result of the platform motions. It is necessary to validate the unsteady aerodynamics to assess the numerical accuracy of coupled aero-hydrodynamics of FOWT. The combined wind-wave condition is consistent with that of mesh convergence study. Figure 9 depicts a comparison of unsteady aerodynamics of FOWT among different numerical methods. Compared with the results from the FAST code and high-fidelity blade-resolved method of Zhou et al. (2022), the power predicted in the present study show good agreement, except that the decrease in power in a wave period is not captured because of the absence of a tower. In terms of thrust, our result shows good consistency with that of Zhou et al., whereas the thrust predicted by the FAST code exhibits a minor difference.

RESULTS AND DISCUSSION

Rotor Power

Figure 10 shows the rotor power of the FOWT for the two yaw operation scenarios, as well as the non-yaw situation. We can clearly observe the change of rotor power with the period of incident regular wave. An interval of insufficient rotor power between
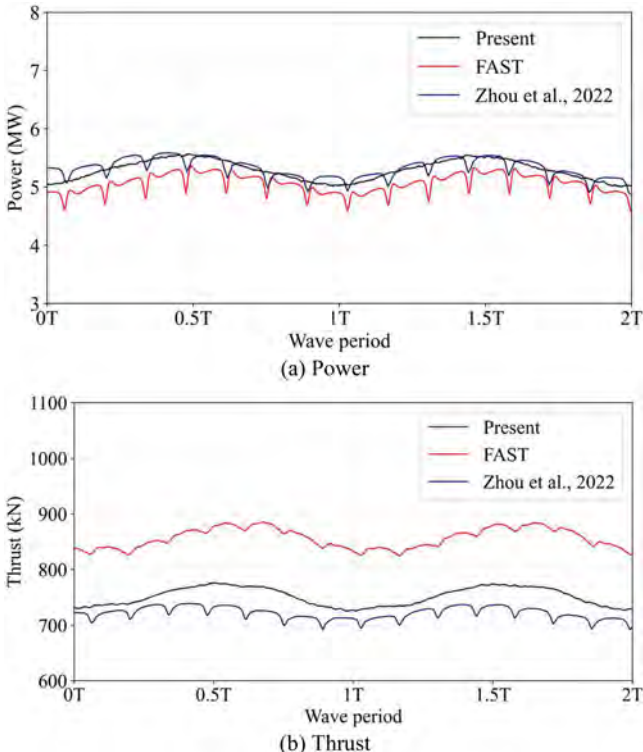

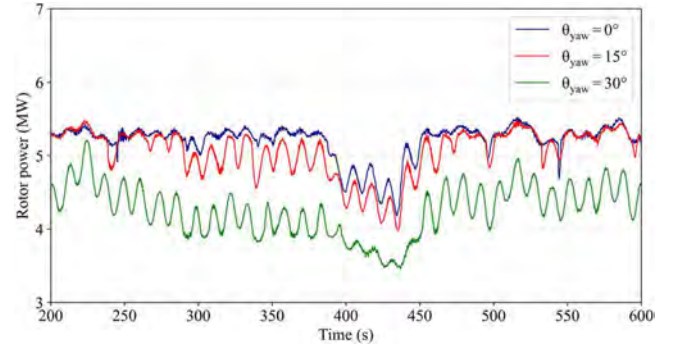Fig. 9 Comparison of unsteady aerodynamic performance of different numerical methods

Fig. 10 Rotor power of the FOWT

Case	Rotor power (MW)				
	Max	Min	Mean	Rms	Std dev
$\theta_{yaw} = 0°$	5.52	4.18	5.20	5.20	0.24
$\theta_{yaw} = 15°$	5.48	3.98	5.06	5.07	0.32
$\theta_{yaw} = 30°$	5.20	3.46	4.26	4.27	0.35

Table 3   Statistics of rotor power of the FOWT

time instants 400 s and 450 s is discernible, possibly because of the large-scale low-speed airflow in the ABL wind field. For the non-yaw scenario, the influence of the incident wave on rotor power is not significant compared with yawed situations. This is attributed to the active blade pitch controller, which regulates the generation of rotor power. When the yaw angle is 15°, the rotor power is slightly decreased because of the reduced windward sweep area of rotor resulting from yaw operation. The reduction in rotor power becomes more conspicuous at the 30° yaw angle.

Apart from the time histories, we present a quantitative analysis of the rotor power of the yawed FOWT, as illustrated in Table 3. The values of maximum, minimum, mean and root mean square (Rms) are decreased when the wind turbine is in the yaw operation, indicating that the yaw operation of the wind turbine can reduce its rotor power. However, for the root mean square of rotor power, the reduced value is 0.13 MW at the 15° yaw angle. Remarkably, this reduction is notably less than the larger
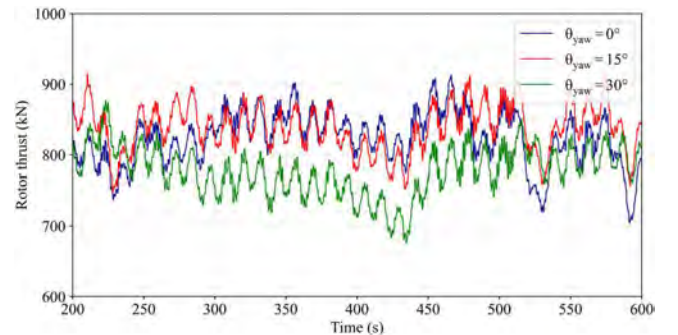

Fig. 11 Rotor thrust of the FOWT

Case	Rotor thrust (kN)				
	Max	Min	Mean	Rms	Std dev
$\theta_{yaw} = 0°$	912.5	704.1	823.9	824.8	38.0
$\theta_{yaw} = 15°$	914.5	748.3	838.1	838.8	33.6
$\theta_{yaw} = 30°$	876.7	675.7	778.0	778.8	34.9

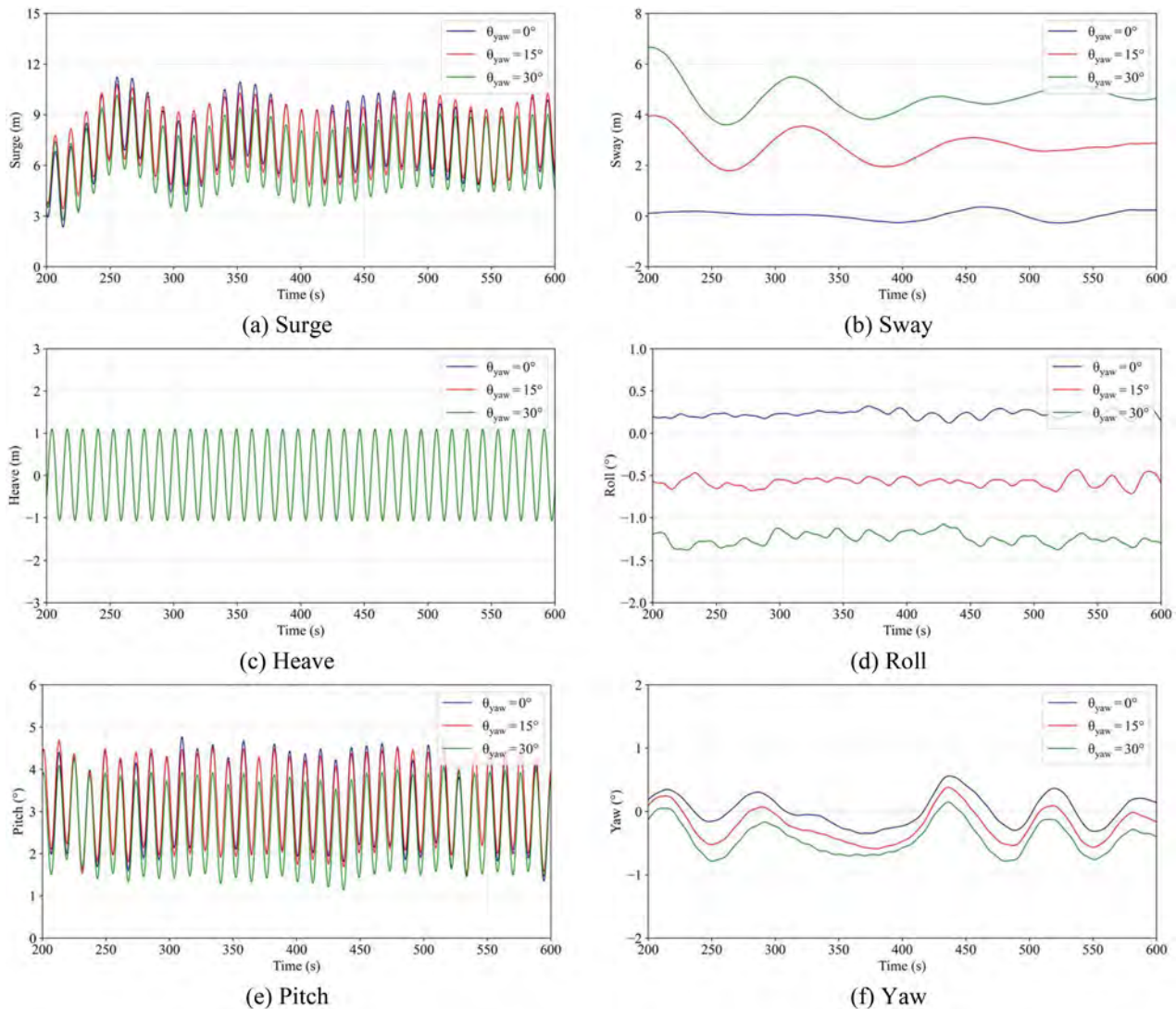Table 4   Statistics of rotor thrust of the FOWT

Fig. 12 Platform motions of the FOWT

decrease of 0.94 MW observed at the 30° yaw angle. This indicates a nonlinear relationship between yaw angle and decrease of rotor power. What's more, the standard deviation of rotor power is enhanced by an increase of yaw angle.

Rotor Thrust

Compared with rotor power, the rotor thrust is also an important parameter for the FOWT. We show the time histories of rotor thrust of the yawed FOWT in Fig. 11. As expected, the rotor thrust of the FOWT oscillates with the period of an incident regular wave, akin to the rotor power behavior discussed earlier. However, we observe an interesting phenomenon where the rotor thrust at the 15° yaw angle is occasionally greater than that of non-yaw scenario. This contrasts with the earlier conclusion that the yaw operation of the wind turbine can reduce its rotor power. According to the definition of the NREL 5MW wind turbine (Jonkman et al., 2009), its rotor thrust first increases and then decreases as the wind speed increases, and the wind speed corresponding to maximum rotor thrust is slightly below 11.4 m/s. The yaw operation of the wind turbine can be equivalent to the reduction of inflow wind speed while maintaining the identical windward sweep area of the rotor as in the non-yaw scenario. Consequently, the rotor thrust with a small yaw angle (i.e., 15°) may be larger

than that of the non-yaw situation when the wind turbine operates under the 11.4 m/s wind speed. However, as the yaw angle increases further, such as the 30° yaw angle, the rotor thrust of FOWT becomes less than that of the non-yaw scenario.

Table 4 illustrates the statistics of rotor thrust of the FOWT. As anticipated, the maximum, minimum, mean, and root mean square (Rms) of rotor thrust under the 15° yaw angle are higher than those of the non-yaw scenario, aligning with the qualitative analysis of rotor power. Specifically, the root mean square of rotor thrust of the 15° yaw angle is 838.8 kN, a slightly enhanced value compared with the 824.8 kN of the non-yaw operation. When the yaw angle is 30°, the above four statistics are decreased because of the significantly reduced windward sweep area of the turbine rotor. In conclusion, it is observed that the rotor thrust of the yawed FOWT does not consistently decrease with an increase of yaw angle. Instead, the rotor thrust is the maximum for a small yaw angle (i.e., 15°).

Platform Motions

Figure 12 illustrates the six-degree-of-freedom motions of the floating platform for the three cases. The regular variations in platform surge, heave, and pitch induced by an incident regular wave are evident. There is no difference in the platform heave motion between the two yaw scenarios and the non-yaw scenario.

The platform surge motion with a 15° yaw angle is occasionally greater than that in the non-yaw condition and occasionally smaller, aligning with the previous analysis of rotor thrust. The rotor thrust of the 15° yaw angle is slightly larger than that in the non-yaw scenario, and the streamwise component of the 15° yaw angle is just slightly below 1. As a result, the streamwise component of rotor thrust of the 15° yaw angle appropriates the rotor thrust of the non-yaw scenario, leading to a minor difference of platform surge motion between the two situations.

Nonetheless, when the yaw angle increases to 30°, a significant decrease of platform surge motion is visualized. A similar conclusion can be drawn for platform pitch motion.

Regarding the other three platform motions—sway, roll, and yaw—the hydrodynamic responses of the floating platform increase with an increase of yaw angle. When the wind turbine operates in a non-yaw condition, these platform motions are generally negligible, especially the platform sway motion. However, in yawed operation, the sway motion of a floating platform is amplified by the crosswise component of rotor thrust, as shown in Fig. 12b. For instance, the platform sway motion under the 30° yaw angle reaches oscillations of 5 m, which diminishes to 3 m when the yaw angle decreases to 15°. For the platform roll and yaw motions, the distinct differences between the two yaw scenarios and non-yaw situation are not observed.

Wind Turbine Wake

Figure 13 shows the time-averaged streamwise velocity contours at the hub height level; note that the contours are averaged using the data of last 400 s. The wake of the wind turbine, characterized by a significant velocity deficit, is clearly visible. Furthermore, the wake widens as it travels downstream. In comparison to the non-yaw scenario, the wake of the wind turbine under the
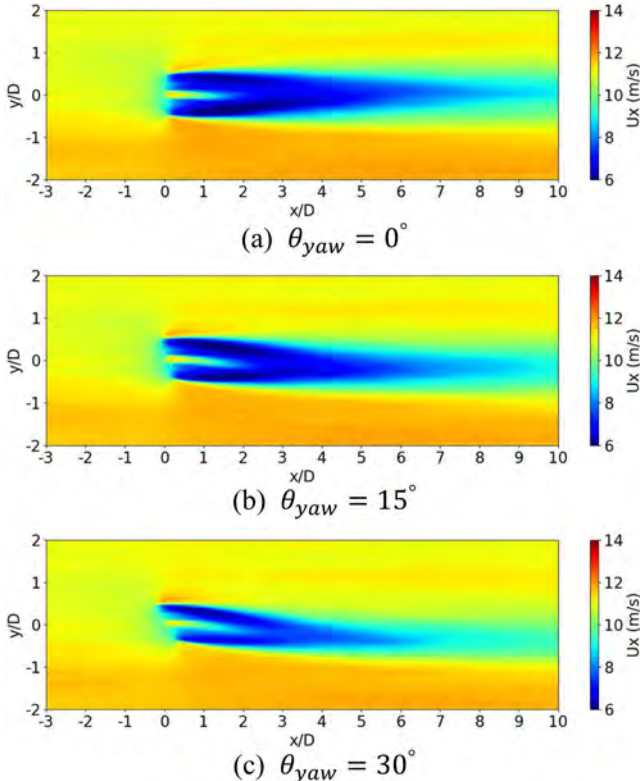

Fig. 13 Time-averaged streamwise velocity contours at the hub height level of FOWT
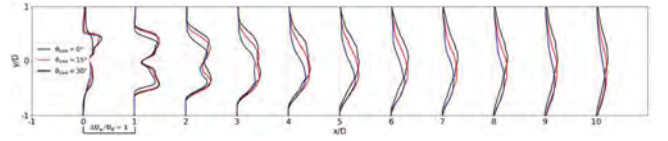

Fig. 14 Time-averaged velocity deficit in a hub-level plane

15° yaw angle deflects to the right when the sight towards downstream, and the deflection is more pronounced with an increase of yaw angle. In addition, we observe faster wake recovery in the yawed condition. The wake of the wind turbine under a non-yaw operation remains apparent at downstream $10D$ ($D = 126$ m is the rotor diameter), whereas this distance is reduced to downstream $9D$ and $7D$ for yaw angles of 15° and 30°. One possible reason for this could be that the crosswise component of velocity induced by the yaw operation of the wind turbine enhances the mixing between an outside ambient flow field and a wind turbine wake. Figure 14 shows the velocity deficit profile in the hub level plane. This quantitative result further supports the conclusions summarized from Fig. 13.

Figure 15 shows the wake center at a hub height level for the three cases, aiming to offer a quantitative insight into the impact of yaw angle on wind turbine wake. Note that the wake center is determined by using the Gauss fitting function. As expected, the wake center of the non-yaw scenario closes to the initial rotor center. For the situations of yaw operation, the wake center deflects away from the initial rotor center, and the deflection is enhanced with a larger yaw angle. For instance, at a downstream distance of $7D$, the wake centers of 15° and 30° yaw angles are approximately $-0.2D$ and $-0.3D$, respectively. In addition, the wake deflection between downstream $4D$ and $6D$ is more pronounced compared with greater downstream distances. This phenomenon can be attributed to the gradual weakening of the crosswise component of velocity's influence on wake deflection as the wake travels further downstream.

Figure 16 shows the time-averaged streamwise velocity contours of a vertical plane at different downstream distances. As shown, the wind velocity near the bottom is lower, which is caused by the friction of the sea surface and numerically implemented by the surface stress model. For the non-yaw scenario, the wake expansion and wake recovery are significantly observed. In line with previous analysis of velocity contours at the hub height level, the wake recovery is faster as the yaw angle increases. In addition to wake recovery, the yaw operation of the wind turbine leads to a wind turbine wake far away from the initial position of the wind turbine rotor, which is beneficial for the inflow wind condition and power generation of downstream wind turbines. Consequently, the yaw control by forcing an upstream wind turbine to operate with a yaw angle may be a potential technique to improve the power generation of a wind farm (Wei et al., 2021).
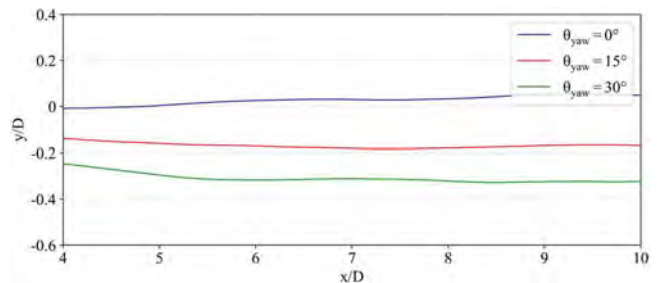

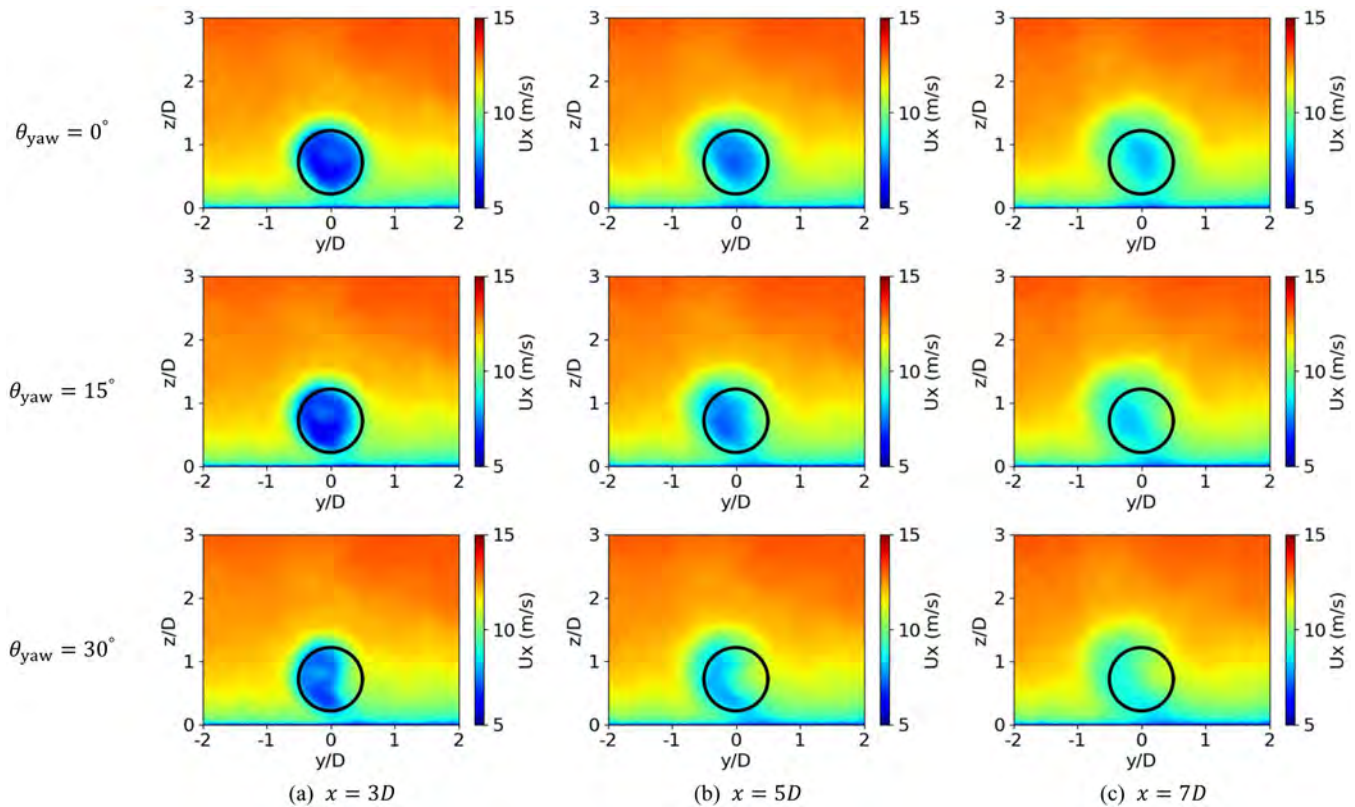Fig. 15 Wake center at hub height level of FOWT

Fig. 16 Time-averaged streamwise velocity contours of vertical plane at different downstream distances of FOWT: Rows denote the contours of different scenarios, and columns (a), (b), and (c) denote downstream $3D$, $5D$, and $7D$, respectively; the blade circle is the initial position of wind turbine rotor.

CONCLUSIONS

In this paper, we present a numerical study of a yawed FOWT immersed in an ABL wind field. The FOWT model is composed of an NREL 5MW wind turbine and the OC4 DeepCWind semisubmersible floating platform. The ABL wind field is simulated and generated by the LES with sufficient simulation duration. The aero-hydro-moor-servo dynamics of FOWT is predicted by NREL FAST code. Two yaw angles of 15° and 30° of wind turbine are performed, and the results of aerodynamics, hydrodynamics, and wake characteristics are compared and analyzed with those of the non-yaw scenario.

It can be concluded that the rotor power of FOWT decreases with an increase of the yaw angle. However, the rotor thrust of a 15° yaw angle is 838.8 kN, which is a slightly enhanced value compared with 824.8 kN of a non-yaw situation. Because the rotor thrust is significantly reduced, the platform surge motion and pitch motion of the 30° yaw angle are smaller than those of the non-yaw scenario. However, the surge and pitch motions of the 15° yaw angle are close to those of the non-yaw scenario, as the rotor thrust is slightly increased and the streamwise component of the 15° yaw angle just slightly below 1. The sway motion of the floating platform is enhanced by the crosswise component of rotor thrust; consequently, the platform sway motion increases with an increase of yaw angle.

For the wake characteristics of the wind turbine, the wake recovery and wake expansion are clearly visible when the wake travels downstream. The faster wake recovery with increase of yaw angle is observed. For instance, the wake under the non-yaw operation is significantly visible at downstream $10D$, whereas this distance is reduced to downstream $9D$ and $7D$ when the yaw angles are 15° and 30°, respectively. What's more, the wake center deflection is more significant with an increase in yaw angle,

which is beneficial for the inflow wind condition and power generation of a downstream wind turbine.

ACKNOWLEDGEMENTS

REFERENCES

Bai, H, Wang, N, and Wan, D (2023). "Numerical Study of Aerodynamic Performance of Horizontal Axis Dual-rotor Wind Turbine Under Atmospheric Boundary Layers," *Ocean Eng*, 280, 114944. https://doi.org/10.1016/j.oceaneng.2023.114944.

Chanprasert, W, Sharma, RN, Cater, JE, and Norris, SE (2022). "Large Eddy Simulation of Wind Turbine Fatigue Loading and Yaw Dynamics Induced by Wake Turbulence," *Renewable Energy*, 190, 208–222.
https://doi.org/10.1016/j.renene.2022.03.097.

Cheng, P, Huang, Y, and Wan, D (2019). "A Numerical Model for Fully Coupled Aero-hydrodynamic Analysis of Floating Offshore Wind Turbine," *Ocean Eng*, 173, 183–196.
https://doi.org/10.1016/j.oceaneng.2018.12.021.

Churchfield, MJ, Lee, S, Michalakes, J, and Moriarty, PJ (2012). "A Numerical Study of the Effects of Atmospheric and Wake Turbulence on Wind Turbine Dynamics," *J Turbul*, (13), N14. https://doi.org/10.1080/14685248.2012.668191.

Churchfield, M, Lee, S, and Moriarty, P (2012). *Overview of the Simulator for Wind Farm Application* (*SOWFA*), National Renewable Energy Laboratory, Golden, CO, USA, 96 pp.

Doubrawa, P, Churchfield, MJ, Godvik, M, and Sirnivas, S (2019). "Load Response of a Floating Wind Turbine to Turbulent Atmospheric Flow," *Appl Energy*, 242, 1588–1599. https://doi.org/10.1016/j.apenergy.2019.01.165.

Huang, Y, and Wan, D (2019). "Investigation of Interference Effects Between Wind Turbine and Spar-type Floating Platform Under Combined Wind-wave Excitation," *Sustainability*, 12(1), 246. https://doi.org/10.3390/su12010246.

Huang, Y, Wan, D, and Hu, C (2021). "Numerical Analysis of Aero-hydrodynamic Responses of Floating Offshore Wind Turbine Considering Blade Deformation," *Proc 31st Int Ocean Polar Eng Conf*, Rhodes, Greece, ISOPE, 1, 450–458.

Jasak, H, Jemcov, A, and Tukovic, Z (2007). "OpenFOAM: A C++ Library for Complex Physics Simulations," *Proc Int Workshop Coupled Methods Numer Dyn*, Dubrovnik, Croatia, IUC Dubrovnik, 1000, 1–20.

Johlas, HM, Martinez-Tossas, LA, Churchfield, MJ, Lackner, MA, and Schmidt, DP (2021). "Floating Platform Effects on Power Generation in Spar and Semisubmersible Wind Turbines," *Wind Energy*, 24(8), 901–916. https://doi.org/10.1002/we.2608.

Jonkman, JM, and Buhl, ML, Jr (2005). *FAST User's Guide*, Technical Report NREL/TP-500-38230, National Renewable Energy Laboratory, Golden, CO, USA, 125 pp.

Jonkman, J, Butterfield, S, Musial, W, and Scott, G (2009). *Definition of a 5-MW Reference Wind Turbine for Offshore System Development*, Technical Report NREL/TP-500-38060, National Renewable Energy Laboratory, Golden, CO, USA, 63 pp.

Li, L, Liu, Y, Yuan, Z, and Gao, Y (2018). "Wind Field Effect on the Power Generation and Aerodynamic Performance of Offshore Floating Wind Turbines," *Energy*, 157, 379–390. https://doi.org/10.1016/j.energy.2018.05.183.

Li, Y, Huang, X, Tee, KF, Li, Q, and Wu, XP (2020). "Comparative Study of Onshore and Offshore Wind Characteristics and Wind Energy Potentials: A Case Study for Southeast Coastal Region of China," *Sustainable Energy Technol Assess*, 39, 100711. https://doi.org/10.1016/j.seta.2020.100711.

National Renewable Energy Laboratory (2022). *FAST v8*, https://www.nrel.gov/wind/nwtc/fastv8.html/ (accessed December 26, 2022).

Ning, X, and Wan, D (2019). "LES Study of Wake Meandering in Different Atmospheric Stabilities and Its Effects on Wind Turbine Aerodynamics," *Sustainability*, 11(24), 6939. https://doi.org/10.3390/su11246939.

Porté-Agel, F, Bastankhah, M, and Shamsoddin, S (2020). "Wind-turbine and Wind-farm Flows: A Review," *Boundary Layer Meteorol*, 174(1), 1–59. https://doi.org/10.1007/s10546-019-00473-0.

Ramachandran, RC, Desmond, C, Judge, F, Serraris, JJ, and Murphy, J (2022). "Floating Wind Turbines: Marine Operations Challenges and Opportunities," *Wind Energy Sci*, 7(2), 903–924. https://doi.org/10.5194/wes-7-903-2022.

Robertson, A, et al. (2014). *Definition of the Semisubmersible Floating System for Phase II of OC4*, Technical Report NREL/TP-5000-60601, National Renewable Energy Laboratory, Golden, CO, USA, 38 pp.

Rohrig, K, et al. (2019). "Powering the 21st Century by Wind Energy—Options, Facts, Figures," *Appl Phys Rev*, 6(3), 031303. https://doi.org/10.1063/1.5089877.

Schumann, U (1975). "Subgrid Scale Model for Finite-difference Simulations of Turbulent Flows in Plane Channels and Annuli," *J Comput Phys*, 18(4), 376–404. https://doi.org/10.1016/0021-9991(75)90093-5.

Smagorinsky, J (1963). "General Circulation Experiments with the Primitive Equations: I. The Basic Experiment," *Mon Weather Rev*, 91(3), 99–164. https://doi.org/10.1175/1520-0493(1963) 091<0099:GCEWTP>2.3.CO;2.

Sørensen, JN, and Shen, WZ (2002). "Numerical Modeling of Wind Turbine Wakes," *J Fluids Eng*, 124(2), 393–399. https://doi.org/10.1115/1.1471361.

Tran, TT, and Kim, DH (2016). "Fully Coupled Aero-hydrodynamic Analysis of a Semi-submersible FOWT Using a Dynamic Fluid Body Interaction Approach," *Renewable Energy*, 92, 244–261. https://doi.org/10.1016/j.renene.2016.02.021.

Troldborg, N (2009). *Actuator Line Modeling of Wind Turbine Wakes*, Doctoral thesis, Technical University of Denmark, 134 pp.

Troldborg, N, Sørensen, JN, and Mikkelsen, R (2007). "Actuator Line Simulation of Wake of Wind Turbine Operating in Turbulent Inflow," *Proc J Phys Conf Ser*, 75(1), 012063. https://doi.org/10.1088/1742-6596/75/1/012063.

Wei, D, Wang, N, Wan, D, and Strijhak, S (2023). "Parametric Study of the Effectiveness of Active Yaw Control Based on Large Eddy Simulation," *Ocean Eng*, 271, 113751. https://doi.org/10.1016/j.oceaneng.2023.113751.

Wei, D, Zhao, W, Wan, D, and Xiao, Q (2021). "A New Method for Simulating Multiple Wind Turbine Wakes Under Yawed Conditions," *Ocean Eng*, 239, 109832. https://doi.org/10.1016/j.oceaneng.2021.109832.

Xu, S, Wang, N, Zhuang, T, Zhao, W, and Wan, D (2023). "Large Eddy Simulations of Wake Flows Around a Floating Offshore Wind Turbine Under Complex Atmospheric Inflows," *Int J Offshore Polar Eng*, ISOPE, 33(1), 1–9. https://doi.org/10.17736/ijope.2023.sv02.

Xu, S, Xue, Y, Zhao, W, and Wan, D (2022). "A Review of High-fidelity Computational Fluid Dynamics for Floating Offshore Wind Turbines," *J Mar Sci Eng*, 10(10), 1357. https://doi.org/10.3390/jmse10101357.

Xu, S, Zhuang, T, Zhao, W, and Wan, D (2023). "Numerical Investigation of Aerodynamic Responses and Wake Characteristics of a Floating Offshore Wind Turbine Under Atmospheric Boundary Layer Inflows," *Ocean Eng*, 279, 114527. https://doi.org/10.1016/j.oceaneng.2023.114527.

Zhang, Y, and Kim, B (2018). "A Fully Coupled Computational Fluid Dynamics Method for Analysis of Semi-submersible Floating Offshore Wind Turbines Under Wind-wave Excitation Conditions Based on OC5 Data," *Appl Sci*, 8(11), 2314. https://doi.org/10.3390/app8112314.

Zhou, Y, et al. (2022). "Exploring Inflow Wind Condition on Floating Offshore Wind Turbine Aerodynamic Characterisation and Platform Motion Prediction Using Blade Resolved CFD Simulation," *Renewable Energy*, 182, 1060–1079. https://doi.org/10.1016/j.renene.2021.11.010.